J|A|C|S
ARTICLES
Published on Web 08/01/2006

Nucleophilic Substitution at Phosphorus ($S_N2@P$): Disappearance and Reappearance of Reaction Barriers

Marc A. van Bochove, Marcel Swart, and F. Matthias Bickelhaupt*

Contribution from the Afdeling Theoretische Chemie, Scheikundig Laboratorium der Vrije Universiteit De Boelelaan 1083, NL-1081 HV Amsterdam, The Netherlands

Received January 27, 2006; E-mail: F.M.Bickelhaupt@few.vu.nl

Abstract: Pentacoordinate phosphorus species play a key role in organic and biological processes. Yet, their nature is still not fully understood, in particular, whether they are stable, intermediate transition *complexes* (TC) or labile transition states (TS). Through systematic, theoretical analyses of elementary $S_N2@C$, $S_N2@Si$, and $S_N2@P$ reactions, we show how increasing the coordination number of the central atom as well as the substituents' steric demand shifts the $S_N2@P$ mechanism stepwise from a single-well potential (with a stable central TC) that is common for substitution at third-period atoms, via a triple-well potential (featuring a pre- and post-TS before and after the central TC), back to the double-well potential (in which pre- and postbarrier merge into one central TS) that is well-known for substitution reactions at carbon. Our results highlight the steric nature of the S_N2 barrier, but they also show how electronic effects modulate the barrier height.

Pentacoordinate phosphorus species play a key role in a wide range of organic and biological processes that involve nucleophilic attack at phosphorus ($S_N2@P$).[1,2] Yet, the nature of these species is still not fully understood, in particular, whether they are intermediate transition *complexes* (TC) or transition states (TS) that principally escape any attempt of detection or isolation.[2,3] This contrasts with the profound understanding of nucleophilic substitution at carbon ($S_N2@C$)[4] and silicon ($S_N2@Si$)[5] and the corresponding pentacoordinate transition species. The archetypal reactions of $X^- + CH_3X$ and $X^- + SiH_3X$ are often employed to illustrate how the reaction profile changes from a double-well potential energy surface (PES), involving a central TS for substitution at a second-period atom ($S_N2@C$), to a single-well PES associated with a stable TC for substitution at the third-period congener ($S_N2@Si$).

To close this gap in our understanding of bimolecular nucleophilic substitution, we have systematically analyzed and compared a series of archetypal $S_N2@C$, $S_N2@Si$, and $S_N2@P$ reactions using the Amsterdam Density Functional (ADF) program with the OLYP and mPBE0KCIS functionals.[6] These approaches were previously shown to agree satisfactorily with highly correlated ab initio benchmarks (vide infra).[5a,7,8] Our analyses reveal that the main factors determining the shape of the PES, i.e., the presence or absence of reaction barriers, are the steric demand of substituents at phosphorus and, to a lesser extent, the nature of the nucleophile and leaving group. In particular, we show how increasing the steric congestion at phosphorus shifts the $S_N2@P$ mechanism stepwise from a single-well potential (with a stable central TC) that is common for substitution at third-period atoms, via a triple-well potential (featuring a pre- and post-TS before and after the central TC), back to the double-well potential (with a central TS) that is well-known for substitution at carbon.

Our model systems cover symmetric ($X = Y$) and asymmetric nucleophilic substitution ($X \neq Y$) at carbon (eq 1), silicon (eq 2), and phosphorus (eqs 3−11), but herein, we focus on the

(1) (a) Skordalakes, E.; Dodson, G. G.; St Clair-Green, D.; Goodwin, C. A.; Scully, M. F.; Hudson, H. R.; Kakkar, V. V.; Deadman, J. J. *J. Mol. Biol.* **2001**, *311*, 549. (b) Omakor, J. E.; Onyido, I.; van Loon, G. W.; Buncel, E. *J. Chem. Soc., Perkin Trans. 2* **2001**, 324. (c) Oivanen, M.; Kuusela, S.; Lönnberg, H. *Chem. Rev.* **1998**, *98*, 961. (d) Perreault, D. M.; Anslyn, E. V. *Angew. Chem.* **1997**, *109*, 470. (e) Denu, J. M.; Lohse, D. L.; Vijayalakshmi, J.; Saper, M. A.; Dixon, J. E. *Proc. Natl. Acad. Sci. U.S.A.* **1996**, *93*, 2493.

(2) (a) Lahiri, S. D.; Zhang, G.; Dunaway-Mariano, D.; Allen, K. N. *Science* **2003**, *299*, 2067. See also: *Science* **2003**, *301*, 1184c and *Science* **2003**, *301*, 1184d. (b) Yliniemela, A.; Uchimaru, T.; Tanabe, K.; Taira, K. *J. Am. Chem. Soc.* **1993**, *115*, 3032. (c) Asubiojo, O. I.; Brauman, J. I.; Levin, R. H. *J. Am. Chem. Soc.* **1977**, *99*, 7707.

(3) Hanes, R. E., Jr.; Lynch, V. M.; Anslyn, E. V.; Dalby, K. N. *Org. Lett.* **2002**, *4*, 201.

(4) (a) Vayner, G.; Houk, K. N.; Jorgensen, W. L.; Brauman, J. I. *J. Am. Chem. Soc.* **2004**, *126*, 9054. (b) Gronert, S. *Acc. Chem. Res.* **2003**, *36*, 848. (c) Laerdahl, J. K.; Uggerud, E. *Int. J. Mass Spectrom.* **2002**, *214*, 277. (d) Chabinyc, M. L.; Craig, S. L.; Regan, C. K.; Brauman, J. I. *Science* **1998**, *279*, 1882. (e) Deng, L.; Branchadell, V.; Ziegler, T. *J. Am. Chem. Soc.* **1994**, *116*, 10645. (f) Shaik, S. S.; Schlegel, H. B.; Wolfe, S. *Theoretical Aspects of Physical Organic Chemistry: The S_N2 Reaction*; Wiley: New York, 1992. (g) Solà, M.; Lledós, A.; Duran, M.; Bertrán, J.; Abboud, J. L. M. *J. Am. Chem. Soc.* **1991**, *113*, 2873. (h) Olmstead, W. N.; Brauman, J. I. *J. Am. Chem. Soc.* **1977**, *99*, 4219.

(5) (a) Bento, A. P.; Solà, M.; Bickelhaupt, F. M. *J. Comput. Chem.* **2005**, *26*, 1497. (b) Windus, T. L.; Gordon, M. S.; Davis, L. P.; Burggraf, L. W. *J. Am. Chem. Soc.* **1994**, *116*, 3568. (c) Gronert, S.; Glaser, R.; Streitwieser, A. *J. Am. Chem. Soc.* **1989**, *111*, 3111. (d) Damrauer, R.; Burggraf, L. W.; Davis, L. P.; Gordon, M. S. *J. Am. Chem. Soc.* **1988**, *110*, 6601.

(6) (a) Baerends, E. J. and co-workers, ADF version 2005.01, SCM, Amsterdam, The Netherlands. (b) te Velde, G.; Bickelhaupt, F. M.; Baerends, E. J.; Fonseca Guerra, C.; van Gisbergen, S. J. A.; Snijders, J. G.; Ziegler, T. *J. Comput. Chem.* **2001**, *22*, 931. (c) Fonseca Guerra, C.; Handgraaf, J.-W.; Baerends, E. J.; Bickelhaupt, F. M. *J. Comput. Chem.* **2004**, *25*, 189. (d) Handy, N. C.; Cohen, A. J. *Mol. Phys.* **2001**, *99*, 403. (e) Lee, C.; Yang, W.; Parr, R. G. *Phys. Rev. B* **1988**, *37*, 785.

(7) (a) Swart, M.; Ehlers, A. W.; Lammertsma, K. *Mol. Phys.* **2004**, *102*, 2467. (b) Baker, J.; Pulay, P. *J. Chem. Phys.* **2002**, *117*, 1441. (c) Xu, X.; Goddard, W. A., III. *J. Phys. Chem. A* **2004**, *108*, 8495. (d) Gonzales, J. M.; Allen, W. D.; Schaefer, H. F., III. *J. Phys. Chem. A* **2005**, *109*, 10613.

(8) Swart, M.; Solà, M.; Bickelhaupt, F. M. *J. Comput. Chem.*, accepted.

10.1021/ja0606529 CCC: $33.50

Table 1. Energies (in kcal/mol) Relative to Reactants of Stationary Points Occurring in S_N2@C, S_N2@Si, and S_N2@P Reactions[a]

			OLYP/TZ2P			OLYP/QZ4P[c]			mPBE0KCIS/QZ4P[d]		
no.	reaction	shape of PES[b]	RC	preTS	TS/TC	RC	preTS	TS/TC	RC	preTS	TS/TC
1a	$Cl^- + CH_3Cl$	double well	−9.0	-	−0.1	−8.1	-	2.1	−9.2	-	3.1
1b	$OH^- + CH_3OH$	double well	−10.2[e]	-	6.2	−8.0[e]	-	10.1	−6.2[e]	-	13.8
2a	$Cl^- + SiH_3Cl$	single well	-	-	−24.4	-	-	−21.8	-	-	−25.7
2b	$OH^- + SiH_3OH$	single well	-	-	−53.8	-	-	−47.5	-	-	−52.2
3a	$Cl^- + PH_2Cl$	single well	-	-	−26.2	-	-	−23.4	-	-	−25.6
3b	$OH^- + PH_2OH$	single well	-	-	−40.2	-	-	−34.7	-	-	−36.8
4a	$Cl^- + POH_2Cl$	single well	-	-	−22.3	-	-	−19.6	-	-	−22.8
4b	$OH^- + POH_2OH$	single well	-	-	−48.8	-	-	−42.3	-	-	−47.6
5a	$Cl^- + PF_2Cl$	single well	-	-	−24.7	-	-	−21.8	-	-	−24.3
5b	$OH^- + PF_2OH$	single well	-	-	−45.5	-	-	−39.4	-	-	−42.6
6a	$Cl^- + POF_2Cl$	single well	-	-	−13.6	-	-	−10.5	-	-	−13.3
6b	$OH^- + POF_2OH$	single well	-	-	−54.2	-	-	−47.1	-	-	−53.0
7a	$Cl^- + PCl_2Cl$	single well	-	-	−23.3	-	-	−20.2	-	-	−22.3
7b	$OH^- + PCl_2OH$	single well	-	-	−52.0	-	-	−46.1	-	-	−49.3
8a	$Cl^- + POCl_2Cl$	triple well	−17.5	−2.0	−8.4	−14.9	−0.9	−5.6	−12.8	−3.4	−9.0
8b	$OH^- + POCl_2OH$	triple well	−34.5	*f*	−58.0[g]	−28.6	*f*	−51.6[g]	−23.3	*f*	−57.2[g]
9a	$Cl^- + P(CH_3)_2Cl$	triple well	−13.0	−12.7	−15.6	−11.2	−10.5	−12.6	−13.8	−13.7	−15.6
9b	$OH^- + P(CH_3)_2OH$	triple well	−28.7 (w)[h]	−26.1 (w)[h]	−32.7	−23.1 (w)[h]	−20.6 (w)[h]	−26.9	−24.7 (w)[h]	−22.4 (w)[h]	−29.6
10a	$Cl^- + PO(CH_3)_2Cl$	double well	−16.2	-	−5.7	−14.2	-	−2.9	−17.2	-	−7.4
10b	$OH^- + PO(CH_3)_2OH$	triple well	−34.3 (w)[h]	−20.6	−33.9	−28.2 (w)[h]	−15.2	−27.0	−30.9 (w)[h]	−18.9	−32.3
11a	$Cl^- + PO(OCH_3)_2Cl$	double well	−14.1	-	2.5	−12.0	-	4.9	−14.7	-	2.0
11b	$OH^- + PO(OCH_3)_2OH$	triple well	−26.3	−18.7	−33.4	−21.5	−12.6	−26.5	−23.6	−16.6	−32.3
11c	$CH_3O^- + PO(OCH_3)_2OCH_3$	triple well	−16.2	−4.6	−11.2	−14.5	−2.6	−8.8	−19.1	−9.4	−17.3

[a] Computed at OLYP/TZ2P; see Figure 1 for selected structures. [b] Shape of potential energy surface: single-well (no TS), double-well (one TS), or triple-well (two TS). [c] Computed at the OLYP/QZ4P//OLYP/TZ2P level. [d] Computed at mPBE0KCIS[post-SCF@OLYP/QZ4P]//OLYP/TZ2P. [e] Labile with respect to forming water−methoxide complex **1bWC**. [f] Not found due to nonconverging SCF. [g] TC along enforced reaction coordinate 8b. This species is however TS for a symmetric frontside S_N2@P substitution of $Cl^- + POCl(OH)_2$ leading to expulsion of Cl^-. [h] Water−carbanion complex "w" formed after barrier-free proton transfer from a methyl substituent to hydroxide.

symmetric reactions for X = Cl (1a−11a), OH (1b−11b), and CH_3O (11c) (Table 1):

$$X^- + CH_3Y \rightarrow CH_3X + Y^- \quad (1)$$

$$X^- + SiH_3Y \rightarrow SiH_3X + Y^- \quad (2)$$

$$X^- + PH_2Y \rightarrow PH_2X + Y^- \quad (3)$$

$$X^- + POH_2Y \rightarrow POH_2X + Y^- \quad (4)$$

$$X^- + PF_2Y \rightarrow PF_2X + Y^- \quad (5)$$

$$X^- + POF_2Y \rightarrow POF_2X + Y^- \quad (6)$$

$$X^- + PCl_2Y \rightarrow PCl_2X + Y^- \quad (7)$$

$$X^- + POCl_2Y \rightarrow POCl_2X + Y^- \quad (8)$$

$$X^- + P(CH_3)_2Y \rightarrow P(CH_3)_2X + Y^- \quad (9)$$

$$X^- + PO(CH_3)_2Y \rightarrow PO(CH_3)_2X + Y^- \quad (10)$$

$$X^- + PO(OCH_3)_2Y \rightarrow PO(OCH_3)_2X + Y^- \quad (11)$$

Results and Discussion

Potential Energy Surfaces. Geometries, potential energy surfaces (PES), and analyses along the reaction coordinates have been computed consistently at OLYP/TZ2P.[6] In our study, it is important that we do not miss a barrier in one of the model reactions. Therefore, we have verified the potential energy surfaces with a basis set (QZ4P)[6] that is close to the basis-set limit using again OLYP and, in addition, the hybrid-functional mPBE0KCIS. This was done in a single-point manner using the OLYP/TZ2P geometries (see Table 1). In a recent benchmarking study on the performance of all classes of DFT approaches for describing S_N2 reactions, OLYP emerged as the best functional for geometries, whereas mPBE0KCIS achieved the best agreement for relative energies as compared to CCSD(T) computations (e.g., mean absolute deviation for S_N2 central barriers of 1.854 kcal/mol).[8] Inspection of the results in Table 1 shows that OLYP/TZ2P indeed tends to somewhat underestimate barriers compared to mPBE0KCIS/QZ4P: by up to 3 kcal/mol for $X^- = Cl^-$ (1a−11a) and by up to 7 kcal/mol for $X^- = OH^-$ (1b−11b). Importantly, however, all features that determine the nature of a model reaction (i.e., the number and relative height of intermediate complexes and transition states) remain the same at any of the three levels of theory. The remainder of the discussion is based on the OLYP/TZ2P computations.

In the case of $X^- = OH^-$ (but not for $X^- = Cl^-$), regular backside nucleophilic substitution is found to compete with facile alternative pathways, notably proton transfer from substrate to the hydroxide anion. For example, the most stable encounter complex of $OH^- + CH_3OH$ is not the direct precursor to S_N2 substitution, i.e., the reactant complex $OH^-\cdots CH_3OH$ (at −10.2 kcal/mol), but a water−methoxide complex (at −38.9 kcal/mol relative to reactants) that is formed through spontaneous proton transfer as OH^- approaches CH_3OH at the frontside. Here, we focus on the regular S_N2 reaction coordinate because, in the present investigation, OH^- is a model for alkoxides RO^-, the structure of which rules out the above side reaction. However, in those instances in which alternative behavior unavoidably merges with the regular S_N2 pathway, e.g., spontaneous proton transfer along the reaction coordinate (vide infra), it is explicitly discussed.

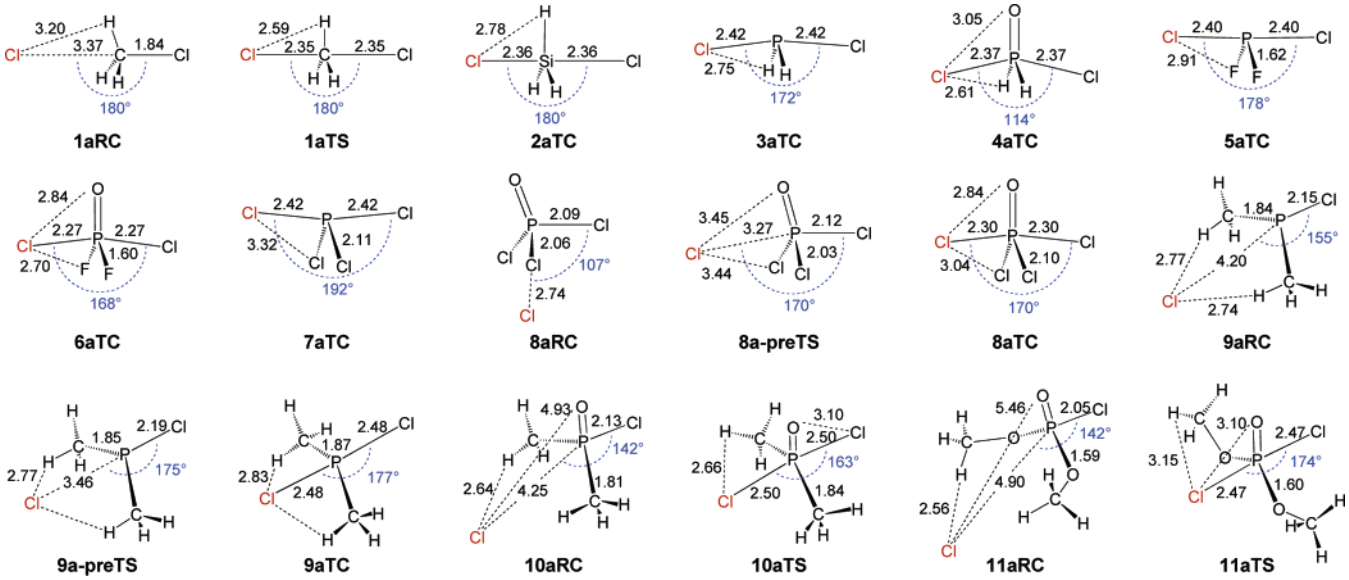

Figure 1. Structures (in Å, deg; at OLYP/TZ2P) of selected stationary points for anionic S_N2@C, S_N2@Si, and S_N2@P reactions.

The characteristics of S_N2@P strongly resemble those of S_N2@Si and not those of S_N2@C as follows, not unexpectedly,[9] from comparing reactions 1−3 (see Table 1 and Figure 1). The usual shift from a double-well PES for S_N2@C to a single-well PES for S_N2@Si is perfectly recovered along reactions 1 and 2. The reactant complexes (RC) in the S_N2@C reactions of Cl^- (1a) and OH^- (1b) are bound by −9.0 and −10.2 kcal/mol, and they are separated from the product complex (PC) by a central barrier of 8.9 and 16.3 kcal/mol, respectively. On the other hand, the S_N2@Si reactions of Cl^- (2a) and OH^- (2b) feature only a stable pentacoordinate TC (no TS, RC, PC) at −24.4 and −53.8 kcal/mol. The corresponding S_N2@P reactions are electronically equivalent (isolobal) to both S_N2@C and S_N2@Si, but they clearly show the behavior of the latter. Thus, going from CH_3X to the isolobal PH_2X, the central S_N2 barrier disappears and the TS turns into a stable pentacoordinate TC, one at −26.2 kcal/mol for Cl^- (3a) and a more stable one at −40.2 kcal/mol for OH^- (3b).

The above shows that archetypal S_N2@P at halophosphines proceeds just as S_N2@Si does, that is, via a single-well PES, with a pronouncedly stable TC instead of a central barrier. This characteristic may however be changed by increasing the steric demand around phosphorus in the transition species, either by increasing the bulk of the substituents themselves or by increasing the coordination number from 4 to 5.[10] This also brings us to the biologically relevant S_N2@P reactions.[1,2] In particular, the (transient) pentacoordinate phosphorus structure has been studied and debated widely.[1−3,10a,b] In many cases, evidence for its existence as a stable intermediate is indirect, i.e., provided through elimination of alternative pathways (see, e.g., the search for a stable hydroxy-phosphorane in ref 3).

Our computations show that either increasing the coordination number (eq 4) or slightly raising the steric bulk of the substituents alone (eq 7) does essentially not change the nature of the reaction profile which remains a single well with a stable TC (see Table 1 and Figure 1). Thus, going from Cl^- attacking tricoordinate PH_2Cl (3a) to Cl^- attacking tetracoordinate POH_2-Cl (4a) somewhat destabilizes the transition species, but it remains a stable TC. The increased stability in the TC from OH^- + PH_2OH (3b) to OH^- + POH_2OH (4b) is caused by intramolecular hydrogen bonding between hydroxy hydrogens and the oxygen substituent (not shown in Figure 1). Likewise, if we replace hydrogen substituents at phosphorus by the more bulky chlorine atoms through going from X^- attacking PH_2X (eq 3) to X^- attacking PCl_2X (eq 7), the transition species for X = Cl is destabilized but it remains an intermediate TC. The TC in the case of X^- = OH^- is again *stabilized* from reaction 3b to 7b due to intramolecular hydrogen bonding, this time between hydroxy hydrogens and the partially negatively charged chlorine substituents (not shown in Figure 1).

Only if the steric bulk of the substituents is further increased by going from chlorine (eq 7) to methyl substituents at phosphorus, i.e., in the reactions of X^- + $P(CH_3)_2X$ (eq 9), we observe a new feature along the PES, namely pre- and post-transition states that surround the transition species (see Table 1). The latter are destabilized for both, X = Cl (9a) and OH (9b), with respect to the corresponding reactions involving chlorine substituents (7a and 7b). But still they remain intermediate TCs, that is, they do not turn into transition states. Note that the pre- and postbarriers separating the reactant and product complexes from the stable TC are relatively small: only 0.3 kcal/mol for X = Cl (9a) and 2.6 kcal/mol for X = OH (9b) (see Table 1). Note also that in the RC and pre-TS of OH^- + $P(CH_3)_2OH$ (9b) spontaneous proton transfer occurs from one of the two methyl groups to the hydroxide anion, leading to the formation of a water−carbanion complex $HO-H\cdots{}^-CH_2-PCH_3OH$ (not shown in Figure 1). This is indicated by the letter "w" in Table 1. The water−carbanion structure persists as the reaction further proceeds to the pre-TS, but as the nucleophile−substrate O−P bond is formed in the symmetric transition

(9) (a) Sølling, T. I.; Pross, A.; Radom, L. *Int. J. Mass Spectrom.* **2001**, *210−211*, 1. (b) Bachrach, S. M.; Mulhearn, D. C. *J. Phys. Chem.* **1993**, *97*, 12229.

(10) (a) Holmes, R. R. *Acc. Chem. Res.* **2004**, *37*, 746. (b) Holmes, R. R. *Chem. Rev.* **1996**, *96*, 927. (c) Chang, N.; Lim, C. *J. Am. Chem. Soc.* **1998**, *120*, 2156. (d) Hengge, A. C.; Onyido, I. *Curr. Org. Chem.* **2005**, *9*, 61. (e) Lum, R. C.; Grabowski, J. J. *J. Am. Chem. Soc.* **1992**, *114*, 8619. (f) Mikolajczyk, M.; Omelanczuk, J.; Perlikowska, W. *Tetrahedron* **1979**, *35*, 1531. (g) Kyba, E. P. *J. Am. Chem. Soc.* **1976**, *98*, 4805. (h) Cook, R. D.; Diebert, C. E.; Schwarz, W.; Turley, P. C.; Haake, P. *J. Am. Chem. Soc.* **1973**, *95*, 8088.

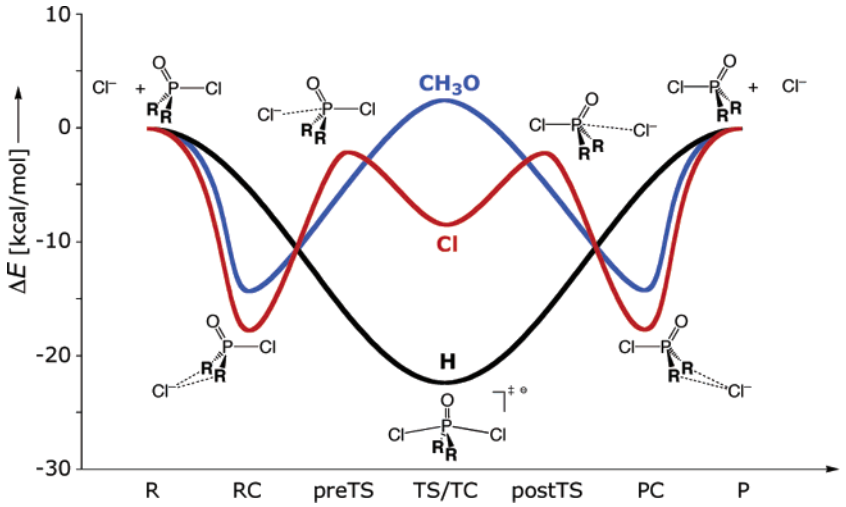

Figure 2. Potential energy surfaces ΔE along the reaction coordinate of the S_N2@P reactions of $Cl^- + POR_2Cl$ for R = H (black), Cl (red), and OCH_3 (blue), computed at OLYP/TZ2P.

complex TC, the proton stemming from the methyl group is returned to the latter.

Interestingly, the *combined* effect of an increased coordination number at phosphorus *and* more bulky chlorine substituents immediately induces a clear, qualitative change in the shape of the reaction profile toward a triple-well PES: going from $X^- + PH_2X$ (eq 3) to $X^- + POCl_2X$ (eq 8), profound pre- and post-transition states arise on the PES. They separate reactant and product complexes from the pentacoordinate transition species. The latter is however still a stable TC. In the case of $Cl^- + POCl_2Cl$ (8a), the preTS is a sizable 15.5 kcal/mol above the RC and, compared to reaction 7a, the central TC is further destabilized, to only −8 kcal/mol relative to the reactants (see Table 1). The central TC of $OH^- + POCl_2OH$ (8b) receives again significant stabilization from intramolecular hydrogen bonding and drops to −58 kcal/mol relative to reactants. Analyses[11,12] reveal that we are witnessing the "lift-off" of pre- and postTSs from the PES due to steric repulsion (Pauli repulsion) between the nucleophile and the substituents around phosphorus. This repulsion partially translates into geometric strain (deformation) which is still present in the central TC, after the steric prebarrier has already been crossed (vide infra).

The most striking effect of increasing the electronegativity of the halogen substituents occurs in the S_N2@P reactions involving the substrates with tetracoordinate phosphorus, i.e., $X^- + POR_2X$. Here, the change from chlorine (eq 8) to the more electronegative fluorine (eq 6) substituents causes the small pre- and postbarriers to disappear again. Furthermore, in the case of $X^- = Cl^-$, the TC is stabilized by −5.2 kcal/mol (compare 8a and 6a in Table 1) in the fluorine-substituted system in which the phosphorus atom is more positively charged, causing a more favorable interaction with the nucleophile. On the other hand, for $X^- = OH^-$, the reduced hydrogen bonding with the more electronegative F substituents causes a destabilization of +3.8 kcal/mol (compare 8b and 6b in Table 1). The same trend in relative stabilities, only less pronounced, is found if one goes from chlorine (eq 7) to fluorine substituents (eq 5) in the S_N2@P reactions involving the substrates with *tri*coordinate phosphorus, i.e., $X^- + PR_2X$ (see Table 1).

Intrigued by the occurrence of barriers in the case of larger substituents, we further increased the steric bulk at tetracoordinate phosphorus through replacing the chlorine substituents (eq 8) by methyl (eq 10) and finally by methoxy groups as they are found in various organic and biological systems (eq 11). Strikingly, with $Cl^- + PO(CH_3)_2Cl$ (10a) and $Cl^- + PO(OCH_3)_2Cl$ (11a), we recover, for the first time, the classical double-well potential for an S_N2 substitution *at a third-period atom*, with real transition states at −5.7 (10a) and +2.5 kcal/mol (11a) relative to the reactants (see Table 1). The analyses[11] show that this originates from a further increase of steric repulsion around the congested pentacoordinate phosphorus (vide infra). Figure 2 illustrates how, along reactions 4a, 8a, and 11a, the increasing steric repulsion first causes the occurrence of steric pre- and postbarriers which eventually merge into one central barrier. The steric factors can be counteracted by strengthening the nucleophile−substrate interaction, e.g., by going from $X^- = Cl^-$ to OH^- (10b, 11b) or to CH_3O^- (11c).[13] This leads to a substantial stabilization of the transition species which become again a stable TC (see Table 1).

Activation Strain Analyses of the Model Reactions. Next, we address the steric nature of the various S_N2 reaction barriers that was already mentioned in the discussion above. The insight that these barriers are in most cases steric emerges from our Activation Strain analyses of the model reactions.[11] The Activation Strain model[11] is a fragment approach to understanding chemical reactions in which the height of reaction barriers is described and understood in terms of the original reactants. Thus, the potential energy surface $\Delta E(\zeta)$ is decomposed, along the reaction coordinate ζ, into the strain $\Delta E_{strain}(\zeta)$ associated

(11) (a) Diefenbach, A.; de Jong, G. Th.; Bickelhaupt, F. M. *J. Chem. Theory Comput.* **2005**, *1*, 286. (b) Diefenbach, A.; Bickelhaupt, F. M. *J. Chem. Phys.* **2001**, *115*, 4030. (c) Bickelhaupt, F. M. *J. Comput. Chem.* **1999**, *20*, 114.

(12) (a) Bickelhaupt, F. M.; Baerends, E. J. In *Reviews in Computational Chemistry*; Lipkowitz, K. B., Boyd, D. B., Eds.; Wiley-VCH: New York, 2000; Vol. 15, pp 1−86. (b) Ziegler, T.; Rauk, A. *Theor. Chim. Acta* **1977**, *46*, 1.

(13) The initially formed TCs for 11b and 11c are not completely symmetric regarding the orientation of the methoxy substituents. Symmetric, ca. 1 kcal/mol more stable TC structures are achieved through flipping one methoxy from the reactant to the product orientation via a small barrier of 1.4 (11b) or 0.4 kcal/mol (11c). Turning the other methoxy substituent also to the product orientation yields a TC that is equivalent to the initial one.

with deforming the individual reactants plus the actual interaction $\Delta E_{int}(\zeta)$ between the deformed reactants (eq 12).

$$\Delta E(\zeta) = \Delta E_{strain}(\zeta) + \Delta E_{int}(\zeta) \quad (12)$$

The strain $\Delta E_{strain}(\zeta)$ is determined by the rigidity of the reactants and on the extent to which groups must reorganize in a particular reaction mechanism, whereas the interaction $\Delta E_{int}(\zeta)$ between the reactants depends on their electronic structure and on how they are mutually oriented as they approach each other. It is the interplay between $\Delta E_{strain}(\zeta)$ and $\Delta E_{int}(\zeta)$ that determines if and at which point along ζ a barrier arises. The activation energy of a reaction $\Delta E^{\neq} = \Delta E(\zeta^{TS})$ consists of the activation strain $\Delta E^{\neq}{}_{strain} = \Delta E_{strain}(\zeta^{TS})$ plus the TS interaction $\Delta E^{\neq}{}_{int} = \Delta E_{int}(\zeta^{TS})$:

$$\Delta E^{\neq} = \Delta E^{\neq}{}_{strain} + \Delta E^{\neq}{}_{int} \quad (13)$$

The interaction $\Delta E_{int}(\zeta)$ between the strained reactants is further analyzed in the conceptual framework provided by the Kohn−Sham molecular orbital (KS-MO) model. To this end, it is further decomposed into three physically meaningful terms:

$$\Delta E_{int}(\zeta) = \Delta V_{elstat} + \Delta E_{Pauli} + \Delta E_{oi} \quad (14)$$

The term ΔV_{elstat} corresponds to the classical electrostatic interaction between the unperturbed charge distributions of the deformed reactants and is usually attractive. The Pauli repulsion ΔE_{Pauli} comprises the destabilizing interactions between occupied orbitals and is responsible for any steric repulsion. The orbital interaction ΔE_{oi} accounts for charge transfer (interaction between occupied orbitals on one moiety with unoccupied orbitals of the other, including the HOMO−LUMO interactions) and polarization (empty−occupied orbital mixing on one fragment due to the presence of another fragment). In the present study, ΔE_{oi} is dominated by the donor−acceptor interactions between the lone-pair orbital of the nucleophile and the empty σ^*_{A-X} orbital (A = central atom, X = leaving group) of the substrate.

The results of the Activation Strain analyses are collected in Figure 3 and Figure S1 in the Supporting Information. In Figure 3, we show, in the left and middle panels, the decomposition of the S_N2 potential energy surfaces $\Delta E(\zeta)$ and, in the right panel, that of the nucleophile−substrate interactions $\Delta E_{int}(\zeta)$ of $Cl^- + CH_3Cl$ (1a), PH_2Cl (3a), POH_2Cl (4a), $PO(CH_3)_2Cl$ (10a). This series is representative for the observed disappearance of the reaction barrier from S_N2@C (1a) to S_N2@P (3a) and the reappearance of a such a barrier for S_N2@P as the steric bulk of substituents at phosphorus increases along reactions 3a, 4a, and 10a.

For each reaction, three situations are analyzed, which are distinguished in the illustrations through a color code: black, blue, and red lines. The black lines refer to the regular internal reaction coordinate (IRC). The IRC is modeled by a linear transit in which the nucleophile−central-atom distance and the central-atom−leaving-group distance run synchronously from their value in the RC to that in the transition structure, TS or TC, in 20 steps. All other geometrical degrees of freedom are fully optimized at each step. In those instances, in which no RC exists, the IRC runs from a geometry that closely resembles the separate reactants ("R") to the TC, where "R" is defined by a nucleophile−central-atom distance of 6 Å and the central-atom−leaving-group distance in the equilibrium structure of the substrate. Next, the analyses represented with blue lines refer to the situation in which the geometry of the substrate is kept frozen to its geometry in the RC (or "R"), except for the central-atom−leaving-group distance and relative orientation; i.e., the $[CH_3]$ or $[POR_2]$ moiety is frozen, but the leaving group still departs as the nucleophile approaches. The red lines, finally, refer to analyses in which the entire substrate is frozen to the geometry it adopts in the RC or to its equilibrium geometry ("R").

First, we examine the S_N2@C reaction of $Cl^- + CH_3Cl$ (1a). As the reaction progresses from the RC to TS, the energy ΔE rises from −9 to 0 kcal/mol (plain black line in Figure 3, left; see also Table 1). In terms of the Activation Strain model, this is so because the stabilization due to the nucleophile−substrate interaction ΔE_{int} cannot compensate the strain ΔE_{strain} that is building up in the substrate.

What causes the substrate strain? And, is there a mechanism that prevents ΔE_{int} from becoming stronger? The nucleophile−substituent (Cl^-−H) distance in **1aTS** is only 2.59 Å, significantly shorter than the 3.20 Å in **1aRC** (see Figure 1). This contact would be even shorter if the H substituents would not bend backward leading to a planar CH_3 moiety in the TS. Indeed, if we freeze $[CH_3]$ in its pyramidal geometry of the RC, the energy ΔE goes up by more than 10 kcal/mol at the TS (compare blue and black lines in Figure 3, left 1a). This is nearly entirely due to a reduction by more than 10 kcal/mol in the nucleophile−substrate interaction ΔE_{int} (blue dashed line, Figure 3, middle 1a). Note that the strain curve is hardly affected. It is only slightly destabilized because, as the leaving group moves away, $[CH_3]$ recovers its intrinsic preference to minimize steric H−H repulsion by adopting a planar geometry[14] (but this is prevented here because $[CH_3]$ is kept frozen in the pyramidal geometry of the RC). The reason that ΔE_{int} is substantially weakened appears to be a substantial rise in steric, that is, Pauli repulsion between the occupied Cl^- 3p AOs and C−H bonding orbitals on CH_3Cl (see rise from black to blue bold lines in Figure 3, right 1a). Both the bonding orbital interactions ΔE_{oi} and the electrostatic attraction ΔV_{elstat} are hardly influenced.

The buildup of substrate strain can only be avoided by completely freezing the substrate to its geometry in the RC, in which case the carbon−leaving-group distance remains fixed at the short value 1.84 Å (see **1aRC** in Figure 1). One might expect the barrier on the PES to collapse as the strain at the TS drops by some 30 kcal/mol to practically[15] zero (see red bold line in Figure 3, middle 1a). But this is not the case. The barrier goes down by only 3 kcal/mol compared to the partially frozen situation! This is because the nucleophile−substrate interaction ΔE_{int} (which is now approximately equal to ΔE) is enormously destabilized and even becomes repulsive near the TS (compare red and blue dashed lines in Figure 3, middle 1a). The reason is not a further increase of the Pauli repulsion which remains practically unchanged (red and blue bold lines nearly coincide in Figure 3, right 1a). This is what one would expect as the steric appearance of the substrate, i.e., the frozen CH_3 moiety, is the same in both simulations. The destabilization in ΔE_{int}

(14) Bickelhaupt, F. M.; Ziegler, T.; Schleyer, P. v. R. *Organometallics* **1996**, *15*, 1477.

(15) ΔE_{strain} is +0.4 and not 0.0 kcal/mol because CH_3Cl is frozen to the geometry it adopts in the RC in which it is already slightly deformed with respect to its own equilibrium structure.

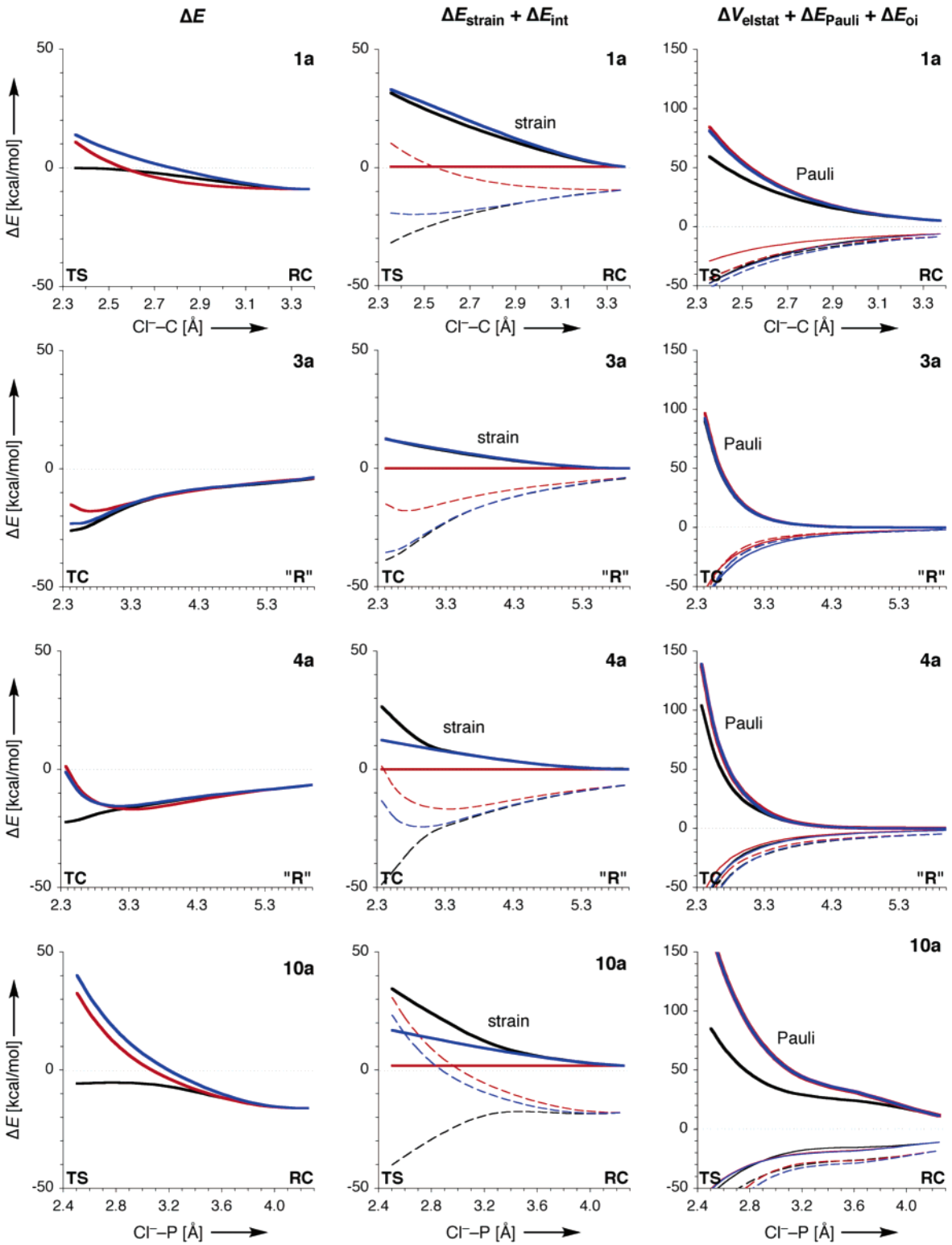

Figure 3. Analysis of the potential energy surfaces ΔE of the S_N2 reactions of $Cl^- + CH_3Cl$ (eq 1a), $Cl^- + PH_2Cl$ (3a), and $Cl^- + POR_2Cl$ for R = H (4a) and CH_3 (10a) along the reaction coordinate projected onto the Cl^-−P (or Cl^-−C) distance. (Left panel) Potential energy surfaces ΔE. (Middle panel) Activation Strain analysis of the potential energy surfaces $\Delta E = \Delta E_{strain}$ (bold lines) + ΔE_{int} (dashed lines). (Right panel) Energy decomposition of the nucleophile−substrate interaction $\Delta E_{int} = \Delta V_{elstat}$ (dashed lines) + ΔE_{Pauli} (bold lines) + ΔE_{oi} (plain lines). (Black lines) Regular internal reaction coordinate (IRC). (Blue lines) IRC with geometry of $[CH_3]$, $[PH_2]$, or $[POR_2]$ unit in substrate frozen to that in the reactant complex (RC) or reactants ("R"). (Red lines) IRC with geometry of entire substrate frozen to that in the RC or "R".

can be traced to a comparable loss in bonding orbital interactions ΔE_{oi} (compare red and blue plain lines in Figure 3, right 1a). The origin is that the donor−acceptor interaction between the Cl^- 3p AO and the CH_3Cl σ^*_{C-Cl} LUMO normally (black but also blue lines) induces an elongation in the carbon−leaving-group bond which amplifies this stabilizing interaction because it leads to a lowering of the σ^*_{C-Cl} orbital and thus a smaller, i.e., more favorable HOMO−LUMO gap. This effect has been

switched off by not allowing the carbon-leaving-group bond to expand. The orbital interactions still increase as the nucleophile approaches because the $<3p|\sigma^*_{C-Cl}>$ overlap increases, but they do so much less efficiently than when the carbon-leaving-group bond is free to expand.

The above analyses demonstrate how the interplay of steric (ΔE_{Pauli}) and electronic factors (ΔE_{oi}) determine the course and barrier height of the S_N2@C reaction. They suggest that by decreasing the steric congestion at the central atom and by strengthening the nucleophile-substrate interaction, one can let the S_N2 barrier disappear. This is exactly what happens if we go from $Cl^- + CH_3Cl$ (1a) to the S_N2@P substitution of $Cl^- + PH_2Cl$ (3a). The TS turns into a stable TC because the strain curve is decimated (from 32 to 13 kcal/mol at the transition structure) and because the interaction becomes 7 kcal/mol more stabilizing (compare 1a and 3a in Figure 3, middle). The $[PH_2]$ moiety is not exposed to a deforming force. Keeping it frozen does not affect the curve of the Pauli repulsion because there is enough space around the tricoordinate phosphorus atom to let the nucleophile attack along a sterically favorable path (black, blue, and red bold lines practically coincide in Figure 3, right 3a). Importantly, the ΔE_{Pauli} curves for $Cl^- + PH_2Cl$ (3a) are over a long trajectory significantly smaller than those of $Cl^- + CH_3Cl$ (1a); only shortly before the TC is reached, they really lift off because of the onset of direct Pauli repulsion with the large phosphorus atom. However, a small central barrier of ca. 3 kcal/mol appears in the fictitious process in which the entire PH_2Cl substrate is kept frozen to its equilibrium geometry (see Figure 3, left 3a). This is again primarily due to reduced donor−acceptor orbital interactions ΔE_{oi} between Cl^- 3p and substrate σ^*_{P-Cl}LUMO (compare red and blue plain lines in Figure 3, right 3a).

The steric congestion at the central atom increases and the situation becomes reminiscent of that of the S_N2@C reaction 1a, as we go from S_N2 at tricoordinate phosphorus in $Cl^- + PH_2Cl$ (3a) to S_N2 at tetracoordinate phosphorus in $Cl^- + POH_2Cl$ (4a). Introducing the extra oxygen substituent tremendously increases the Pauli repulsion ΔE_{Pauli} in the fictitious process in which the $[POH_2]$ moiety is kept frozen pyramidal if compared to the corresponding process with a frozen $[PH_2]$ unit in reaction 3a (compare blue bold lines in Figure 3, right 4a vs 3a). Pauli repulsion is converted into substrate strain in the real S_N2@P process 4a, in which the substrate deformation is not suppressed (compare black and blue bold lines in Figure 3, middle and right 4a). Thus, from reaction 3a to 4a, the strain at the TC increases strongly from 13 to 27 kcal/mol. This is partially counteracted by a more favorable nucleophile−substrate interaction ΔE_{int}, which increases from −39 to −49 kcal/mol, with the more positively charged phosphorus in POH_2Cl. After all, from reaction 3a to 4a, the TC is only slightly destabilized, from −26 to −22 kcal/mol (see Table 1).

Finally, going from hydrogen substituents in $Cl^- + POH_2Cl$ (4a) to methyl substituents in $Cl^- + PO(CH_3)_2Cl$ (10a), the steric bulk becomes sufficiently large to outweigh the favorable nucleophile−substrate interaction and to bring back the double-well potential with a central S_N2 barrier. The Pauli repulsion ΔE_{Pauli} in the fictitious process in which the $[POR_2]$ moieties are kept frozen pyramidal jumps from 139 (4a) to 166 kcal/mol (10a) at the transition structure (in fact, it runs off the scale in the illustration: compare blue bold lines in Figure 3, right 10a vs 4a). The increased Pauli repulsion translates again into a higher strain energy in the real, unconstrained S_N2@P reaction 10a (Figure 3, middle 10a). The nucleophile−substrate interaction does not change that much from 4a to 10a. Thus, the increased steric bulk forces the central reaction barrier to reappear in this S_N2@P substitution. The effects are somewhat more pronounced for the S_N2@P reaction involving the methoxy substituents (see 11a in Figure S1, and Table 1).

Conclusions

The central barrier in S_N2 reactions is determined by the interplay of steric (Pauli repulsion) and electronic effects (e.g., donor−acceptor orbital interactions). From S_N2@C in $Cl^- + CH_3Cl$ to S_N2@P in $Cl^- + PH_2Cl$, the central barrier disappears because there is less steric congestion and a more favorable interaction. But the central barrier reappears as the steric bulk around the phosphorus atom is raised along the model reactions $Cl^- + POH_2Cl$, $PO(CH_3)_2Cl$, and $PO(OCH_3)_2Cl$. Our results highlight the steric nature of the S_N2 barrier.[16]

Acknowledgment. We thank the Netherlands Organization for Scientific Research (NWO-CW) and the National Research School Combination-Catalysis (NRSC-C) for financial support. We also thank the reviewers for valuable comments.

Supporting Information Available: Total energies and Cartesian coordinates of all species occurring in our model reactions, and additional analyses. This material is available free of charge via the Internet at http://pubs.acs.org.

JA0606529

(16) For the role of steric repulsion in determining equilibrium geometries, see also refs 11a, 13, and: Bickelhaupt, F. M.; DeKock, R. L.; Baerends, E. J. *J. Am. Chem. Soc.* **2002**, *124*, 1500.